Biomedicine & Pharmacotherapy 174 (2024) 116449

Contents lists available at ScienceDirect

Biomedicine & Pharmacotherapy

journal homepage: www.elsevier.com/locate/biopha

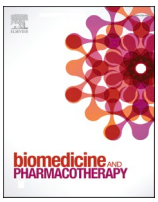

Genipin crosslinking promotes biomechanical reinforcement and pro-regenerative macrophage polarization in bioartificial tubular substitutes

Jone Berasain [a,b], Paula Ávila-Fernández [a,c], Rocío Cárdenas-Pérez [a,b], Antoni Ignasi Cànaves-Llabrés [a,b], Miguel Etayo-Escanilla [a,c], Miguel Alaminos [a,c], Víctor Carriel [a,c], Óscar Darío García-García [a,c,*], Jesús Chato-Astrain [a,c,*], Fernando Campos [a,c]

[a] Tissue Engineering Group, Department of Histology, Faculty of Medicine, University of Granada, Spain
[b] Postgraduate Master Program in Tissue Engineering and Advanced Therapies, University of Granada, Spain
[c] Instituto de Investigación Biosanitaria ibs.GRANADA, Spain

ARTICLE INFO

Keywords:
Peripheral nerve
Fibrin-agarose
Genipin
Biomechanical properties
Macrophage polarization
Anti-inflammatory response

ABSTRACT

Traumatic nerve injuries are nowadays a significant clinical challenge and new substitutes with adequate biological and mechanical properties are in need. In this context, fibrin-agarose hydrogels (FA) have shown the possibility to generate tubular scaffolds with promising results for nerve repair. However, to be clinically viable, these scaffolds need to possess enhanced mechanical properties. In this line, genipin (GP) crosslinking has demonstrated to improve biomechanical properties with good biological properties compared to other crosslinkers. In this study, we evaluated the impact of different GP concentrations (0.05, 0.1 and 0.2% (m/v)) and reaction times (6, 12, 24, 72 h) on bioartificial nerve substitutes (BNS) consisting of nanostructured FA scaffolds. First, crosslinked BNS were studied histologically, ultrastructurally and biomechanically and then, its biocompatibility and immunomodulatory effects were ex vivo assessed with a macrophage cell line. Results showed that GP was able to improve the biomechanical resistance of BNS, which were dependent on both the GP treatment time and concentration without altering the structure. Moreover, biocompatibility analyses on macrophages confirmed high cell viability and a minimal reduction of their metabolic activity by WST-1. In addition, GP-crosslinked BNS effectively directed macrophage polarization from a pro-inflammatory (M1) towards a pro-regenerative (M2) phenotype, which was in line with the cytokines release profile. In conclusion, this study considers time and dose-dependent effects of GP in FA substitutes which exhibited increased biomechanical properties while reducing immunogenicity and promoting pro-regenerative macrophage shift. These tubular substitutes could be useful for nerve application or even other tissue engineering applications such as urethra.

1. Introduction

With an estimated incidence of 300,000 new cases per year in Europe, peripheral nerve damage can frequently appear as a consequence of traumatic injuries, and represent a significant burden for healthcare systems [1–3]. These injuries can result from mechanical, chemical, or thermal trauma, leading to a gap in the nerve structure and subsequent loss of innervation of the target organ [1]. The nerve regeneration process is influenced by various factors, including the patient's biological status, the mechanism of injury, and the severity of the damage [4]. Despite advancements in understanding the physiological mechanisms of nerve regeneration over the past few decades, clinical treatments have not shown significant improvements, and the overall clinical outcome remains unsatisfactory [5]. The current approaches using autografts and allografts have limitations, including donor site morbidity and the risk of immune rejection, warranting the development of innovative biomaterials for nerve repair [3,6].

To successfully generate an artificial nerve substitute able to promote nerve regeneration, essential criteria must be accomplished including biodegradability, porosity, 3D organization, alignment, pro-

* Correspondence to: Department of Histology, Faculty of Medicine, University of Granada, Av. de la Investigación nº11, Building A, 5th floor, Granada CP:18016, Spain.
E-mail addresses: ogarcia@ugr.es (Ó.D. García-García), jchato@ugr.es (J. Chato-Astrain).

https://doi.org/10.1016/j.biopha.2024.116449
Received 9 January 2024; Received in revised form 7 March 2024; Accepted 15 March 2024
Available online 21 March 2024

regenerative chemical composition, and physicochemical properties [3,7]. All these factors play a crucial role in clinically repairing the nerve gap and in stimulating Schwann cells growth at the injury site to support and guide the axonal regeneration process [5,8]. However, and despite the current research and the recent clinical use of several types of nerve substitutes approved by different Medicines Agencies [9], the ideal nerve substitute is still in need. In addition, the generation of tubular tissular substitutes is challenging and novel biofabrication methods allowing generation of cylindrical conduits and tubular shape structures useful in urethra and nerve tissue engineering are in need.

Fibrin-agarose hydrogels (FA) have shown promising clinical results in patients [10,11]. FA demonstrated to act as idoneous scaffolds for the generation of several types of human bioartificial tissues, including the peripheral nerve, showing good biocompatibility, biodegradability, and ability to support cell adhesion and proliferation [12,13]. Bioartificial nerve substitutes (BNS) based on FA efficiently improved nerve regeneration in animal models of sciatic nerve injury [14]. However, to be clinically viable, these scaffolds need to possess enhanced mechanical properties able to withstand the mechanical stresses and strains experienced during the healing process, which could be achieved using non-toxic crosslinking agents [15]. Furthermore, BNS should be able to support a pro-regenerative immune response once grafted into the recipient.

Among the different crosslinking agents used in tissue engineering, genipin (GP) emerged as a promising alternative to the use of glutaraldehyde to enhance the biomechanical properties of biomaterials with reduced cytotoxicity effects [16,17]. GP has been used to successfully crosslink different biomaterials and hydrogels [18] like chitosan [19], collagen [20], as well as decellularized extracellular matrices of nerves [21], cornea [22], or the spinal cord [23], among others. In fact, we previously demonstrated that GP can be successfully used to improve the structural and biomechanical properties of FA hydrogels [24] with adequate *ex vivo* and *in vivo* results [25,26]. In addition, GP has been reported to possess anti-inflammatory properties that may contribute to its low cytotoxicity and could support a pro-regenerative immune response [27,28].

Despite the increasing interest in GP crosslinking in tissue engineering, it is still necessary to determine the impact of the treatment time and dose-dependent effects of GP on the biomechanical and immunological properties of FA-based BNS for nerve repair. The present study aims to evaluate the impact of GP crosslinking fibrin-agarose based BNS, on the biomechanical reinforcement and in its ability to modulate macrophage polarization *ex vivo*.

2. Materials and methods

2.1. Generation of 6-well square plates by 3D-printing

Square-shaped hydrogels were generated using a 6-well plate specifically designed for this purpose. The use of these plates contributed to ensuring consistent density throughout the samples generated in this work. By using the AutoCAD platform and a fused filament printer, squared-shaped plates were fabricated with poly(lactic acid) (PLA) and polyethylene terephthalate glycol (PETG) filaments (Supplementary Figure 1). Each well had a square surface of 3 ×3 cm. After 3D-printing, chloroform treatment was used to enhance interlayer adhesion, reduce porosity, and improve surface texture. Finally, a combination of ethanol and UV rays treatments was used to ensure sterility.

2.2. Generation of bioartificial nerve substitutes

Fibrin-agarose hydrogels (FA) were produced as described in previous studies [29,30]. In brief, to generate 1 mL of hydrogel, the following components were combined and gently mixed: 760 μL of human plasma, 75 μL of DMEM culture medium, 15 μL of tranexamic acid (Amchafibrin, Fides-Ecofarma, Valencia, Spain), 50 μL of a 2% solution of type VII agarose (Merck, Darmstadt, Germany) melted in phosphate-buffered saline (PBS, Merck), and 50 μL of 2% $CaCl_2$ (Merck). Then, 5 mL of the resulting mixture were poured into each well of the 3D printed 6-well plates and allowed to polymerize using standard culture conditions (37°C and 5% CO_2).

Previously described protocols [13,14] were used to produce bioartificial nerve substitutes (BNS). Briefly, hydrogels were carefully removed from the well plates and subjected to plastic compression nanostructuration methods. Squared-shaped FA hydrogels were placed between two nylon filter membranes with a pore size of 0.22 μm (Merck-Millipore, Darmstadt, Germany) and compressed between two sterile Whatman 3 mm absorbent pieces of paper placed below a flat glass surface. A uniform mechanical pressure of 500 g, was applied for 2.5 min, resulting in a high-density nanostructured FA hydrogel. Finally, BNS were generated by carefully rolling nanostructured hydrogels to form concentrical multilayered cylinders measuring 1.5 cm in length and approximately 1.5 mm in diameter, with a thickness of each FA layer of 50–60 μm.

2.3. Genipin-based crosslinking and experimental groups

To improve the structural and biomechanical properties of BNS, constructs were subjected to chemical crosslinking with GP. In this study, twelve experimental groups (n=6) were defined based on three GP concentrations (0.05%, 0.1% and 0.2% (w/v)) and four crosslinking-reaction times (6, 12, 24 and 72 h). Not crosslinked (NGP) BNS were used as controls.

For the crosslinking reaction, we followed previously described protocols [24]. Briefly, constructs were submerged in 10 mL of sterile-filtered GP solutions buffered in PBS (0.1 M, pH 7.2–7.4) at 37°C protected from light. After crosslinking reaction, BNS were washed for 24 h in PBS at 4°C (5 times) to finally obtain GP crosslinked-BNS.

2.4. Macroscopic and microscopic evaluation of bioartificial nerve substitutes

BNS were first photographed and the changes of color intensity after crosslinking reaction were quantified with ImageJ software (version 1.53k, National Institutes of Health, Bethesda, MD, USA) using ten points in three different samples (n=3) of each group as previously described [3,31]. Then, results were normalized to not crosslinked substitutes.

After that, samples (n=3) were subjected to histological analysis for a complete structural characterization. Histological samples were cut in 20 mm long fragments and fixed in 4% buffered formaldehyde solution for 24 h at 4°C. Then, samples were dehydrated, cleared, embedded in paraffin, and sections of 4 μm were obtained following routine histological protocols. Tissue sections were stained with haematoxylin and eosin (H&E) and microscopically evaluated.

Standard protocol was used for scanning electron microscopy (SEM) analysis [32]. 1 mm-long fragments (n=3) were fixed in a 2.5% glutaraldehyde solution in 0.05 M cacodylate buffer (pH 7.2) for 4 h, at 4°C. Fixed samples were washed in cacodylate buffer, dehydrated in increasing alcohol series, and subjected to the critical point drying method. Dried samples were mounted, sputter covered with gold, and analysed using an FEI Quanta 200 scanning electron microscopy (FEI Europe, Eindhoven, Netherlands).

2.5. Biomechanical analysis

To investigate the impact of GP crosslinking on the biomechanical properties of each BNS, samples were subjected to tensile tests (n=6) using an electromechanical testing instrument (Instron, Model 3345-K3327) [13,30,33]. In this experiment, samples were oriented with their length along the direction of tension and clamped at each end, leaving a constant distance of 0.5 cm between the clamps. The tests were

conducted at room temperature with a constant strain rate of 5 mm/min and a 50-N Instron load cell to obtain the data for the stress-strain curves. Instron Blue Hill 2 Material Testing software was used to calculate the Young's modulus (by determining the tangent modulus of the initial linear section of the stress-strain curve for each experimental run), the strain at fracture (by identifying the point on the stress-strain curve where fracture occurred) and the percentage of deformation (automatically calculated based on the elongation before the fracture).

2.6. Ex vivo biocompatibility

2.6.1. Cell culture and biomaterial interaction

The mouse macrophage cell line RAW264.7 was obtained from the American Type Culture Collection (ATTCC) (Manassas, VA, USA). Cells were grown in Dulbecco's Modified Eagle Medium (DMEM) enriched with 10% foetal bovine serum (FBS) and 1% of a penicillin-streptomycin mixture (50 IU/mL) (all from Sigma-Aldrich/Merck, Burlington, MA, USA) and kept in a cell incubator using standard cell culture conditions (37°C and 5% CO_2).

For macrophage biocompatibility tests, macrophages were first seeded in 24-well plates at a density of 6×10^4 cells/cm^2 and allowed to attach to the bottom of the culture surface. Then, each type of BNS (n=6) with a length of 2 mm was allocated on 6.5 mm-diameter porous inserts (Sarstedt, Nümbrecht, Germany), which were placed on each well to allow indirect contact between the cells and the BNS for 24 h. No BNS was used in the control group of undifferentiated macrophages (M0), additionally, bacterial lipopolysaccharide endotoxin (LPS) at a concentration of 0.01 μg/mL (Sigma-Aldrich/Merck) was used in the control group of proinflammatory macrophages (M1).

Then, to assess the *ex vivo* biocompatibility of GP-crosslinked BNS in human cells, we exposed human skin fibroblasts to GP-crossliked BNS at the highest GP concentration (BNS GP 0.2%). Fibroblasts from healthy donors were obtained from skin biopsies and cultured according to established protocols [24] using Dulbecco's Modified Eagle Medium supplemented with 5% antibiotic cocktail solution and 10% fetal bovine serum (Sigma-Aldrich, Germany). To evaluate *ex vivo* biocompatibility, cells were seeded onto each BNS at a density of 5.26×10^3 cells/cm^2, cultured for 48 h under standard conditions, and subsequently subjected to cell viability tests at 3 and 7 days.

2.6.2. Cell viability and proliferation assays

To assess cell viability, LIVE/DEAD Viability/Cytotoxicity kit (Life Technologies, Carlsbad, California, USA) was employed following manufacturer recommendations. In short, cells in contact with the different BNS (n=6 per group) were washed twice with PBS and exposed to the LIVE/DEAD reagent for 5 min at 37°C, protected from light. Subsequently, images were captured utilizing a ZOE Fluorescent Cell Imager (Bio-Rad, Hercules, CA, USA) where viable (green fluorescence) and dead (red fluorescence) cells were identified and the percentage of live cells was calculated. Cells treated with 70% alcohol were used as a technical negative control group (CTR-).

The metabolic activity of cells in indirect contact with the different BNS (n=6 per group) was evaluated by using the Cell Proliferation Reagent WST-1 (Roche, Basel, Switzerland). Briefly, cells were washed twice in PBS and a water-soluble tetrazolium salt reagent (WST-1) was added to each well following the protocols provided by the manufacturer and incubated at 37°C for 2 h. The absorbance of the resulting formazan product was read with an ASYS UVM-340 microplate reader (Biochrom, Cambridge, UK) which correlates with the percentage of metabolically active cells. As positive controls, cells cultured without BNS were used. For the negative control group (CTR-), cells were previously treated with triton X-100 (Sigma-Aldrich). Finally, results were normalized with the negative and positive control groups considered as 0% and 100% of metabolic activity, respectively.

2.6.3. Macrophage phenotypic change analysis

Flow cytometry was used to detect proinflammatory (CD86) or proregenerative (CD163) surface markers on cultured macrophages [34]. In brief, macrophages were incubated with BNS as described in 2.6.1 section, and after biomaterial interaction, cells were detached form the culture wells (n=6 per group), washed twice with PBS and centrifuged at 200 rpm for 5 min. Cell pellets were resuspended in 100 μl of a casein solution with FITC anti-mouse CD86 (0.25 μl) and PE anti-mouse CD163 (0.5 μl) antibodies (both from Thermo Scientific, Waltham, MA, USA) and incubated for 30 min on ice in the dark. Cells were then centrifuged at 200 rpm for 5 min and resuspended in 300 μl PBS and were analyzed using a NovoCyte Flow Cytometer (ACEA Biosciences, San Diego, CA, USA). Cytometric measurements were performed using a laser scanning cytometer. The excitation wavelength was 488 nm. Green (FITC) and red (PE) fluorescence were measured by separate photomultipliers within 530 ± 30 nm and 572 ± 28 nm spectral ranges, respectively. At least 10,000 cells were analyzed per sample. Cells were gated based on their FSC and SSC properties to exclude debris and aggregates and then we used a fluorescence minus one (FMO) control to draw gates around the populations of interest on the FITC and PE channels to distinguish positive from negative events. The percentage of cells showing positive signal for CD86 and CD163 was determined in each experimental group.

2.6.4. Analysis of cytokines released by cells incubated with BNS

In the present study, we quantified several relevant cytokines released to the culture medium by macrophages incubated in the presence of 0.2% GP crosslinked BNS. This concentration was selected, as the highest concentration of GP is expected to exert the most intense immunogenic effects on the cultured cells. As controls, we also analyzed the same cytokines in cells cultured with NGP and in M1 and M0 macrophages. In all these cases, 40 relevant cytokines released by the culture medium were quantified using the Proteome Profiler™ Mouse Cytokine Array Kit (Panel A, ARY006) (R&D Systems, Inc. Minneapolis, USA) by following the manufacturer's instructions. In brief, 50 μl of the culture medium was harvested, and particulates were removed by centrifugation. Then membranes were blocked and incubated with sample medium overnight. Finally, membranes were washed, incubated with streptavidin-HRP and exposed to X-ray films. Array images were then quantified with ImageJ software (version 1.53k, National Institutes of Health, Bethesda, MD, USA) and results were normalized to positive and negative technical controls included in the array [35].

2.7. Quantitative and statistical analyses

For each variable, averages and standard deviations were calculated for each specific group. Then, we calculated the averages and standard deviations of global groups of samples in order to globally evaluate the effects of the GP concentration (all samples subjected to the same GP concentration, regardless the crosslinking reaction time) or the incubation time (all samples subjected to the same GP reaction time, regardless the crosslinking concentration).

For the statistical comparison among groups, each variable was analyzed using the Shapiro-Wilk Test to determine the normality of each distribution. As the distributions analyzed here did not fulfill the normality and parametricity criteria, the non-parametric statistical tests of Kruskal-Wallis and Mann-Whitney were used. In addition, the Kendall's tau correlation test was used to determine the correlation between two specific variables (for example, between the biomechanical properties and macrophage phenotype). For all statistical calculations, a p value below 0.05 was considered statistically significant using two-tailed tests. Statistical comparisons were performed using the Real Statistics Resource Pack software (Release 7.2) (Dr. Charles Zaiontz, Purdue University, West Lafayette, IN, USA), available at www.real-statistics.com.

Finally, in order to explore the variations in the cytokine expression

profile, we conducted a hierarchical clustering analysis of multivariate data using the ClustVis web tool, accessible at https://biit.cs.ut.ee/clustvis/ [36]. Briefly, the average results of each cytokine expression analysis were examined by calculating the correlational distance measure, and the complete clustering method to both the rows and columns of the data.

3. Results

3.1. Macroscopic and microscopic characterization of genipin-crosslinked bioartificial nerve substitutes

The structural characterization of the BNS was carried out by both macroscopic and microscopic evaluations, providing information about their general structure, shape, and internal composition. Macroscopy revealed distinct color changes in the BNS following GP crosslinking as compared with the NGP control group, with a notable blue hue that showed to be influenced in correlation by both the reaction time ($r=0.74$, $p<0.05$) and GP concentration ($r=0.35$, $p<0.05$) (Fig. 1A-B and Supplementary Table S1). Analysis of the BNS using SEM demonstrated uniformity and cohesion across the layers of the substitutes with no detectable changes in structural features after GP reaction (Fig. 1B). Additionally, the histological analysis using H&E staining showed a correlation between color intensity and crosslinking time and concentration, and confirmed that the BNS were composed in all cases of concentrically organized layers of biomaterials, consisting of a fibrillar and well-organized material (Fig. 1C).

3.2. Biomechanical characterization

To analyze the biomechanical properties of BNS crosslinked with GP, a traction tensile test was performed. Biomechanical results are summarized in Fig. 2 and Supplementary Table S2.

First, when studying the global groups regarding GP reaction time (Fig. 2A), it was observed that GP had a significant impact on the biomechanical behaviour of the BNS. Specifically, the Young's modulus was higher in GP crosslinked samples as compared to NGP and increased with the reaction time, being these differences statistically significant at all reaction times ($p<0.05$, Supplementary Table S2). The Young's modulus values increased until 24 h of GP reaction, and significantly decreased afterwards as compared to the 24-h mark ($p = 0.031$, Supplementary Table S2). The correlation between the Young's modulus and the crosslinking reaction time was non-significant ($r=0.08$,$p>0.05$). Moreover, BNS deformation percentage, an indicator of material flexibility, was significantly reduced at all GP reaction times as compared to NGP (Fig. 2A, $p<0.05$, Supplementary Table S2). Additionally, the stress at fracture was reduced after GP treatment but differences were statistically significant only at 6 h ($p = 0.04$, Supplementary Table S2). This parameter followed a similar trend to the Young's modulus, with GP-treated BNS displaying higher values at 24 h and then decreasing at 72 h.

Moving on to the global groups regarding GP concentration (Fig. 2B), we first observed that the GP concentration influenced the biomechanical features of the BNS, as expected. In fact, all GP-treated BNS exhibited higher Young's modulus values than NGP ($p<0.05$, Supplementary Table S2). In this case, the biomechanical parameters were positively modified in a concentration-dependent manner, showing a positive correlation between the Young's modulus and the GP concentration ($r=0.29$, $p<0.05$). On the contrary, an increase in the GP concentration caused a reduced deformation and stress at fracture in the GP-treated BNS, displaying a negative correlation with the GP concentration ($r=-0.31$ and -0.18, respectively, $p<0.05$). More specifically, GP-treated BNS deformation was more intensely influenced by the GP concentration than the stress at fracture, and all GP concentrations showed statistically significant differences with NGP ($p<0.001$, Supplementary Table S2). Conversely, only the highest concentrations of GP (0.1% and 0.2%) showed statistically significant differences with NGP for the stress at fracture.

Finally, the analysis of specific groups of samples (Fig. 1C) revealed that the combination of GP concentration and reaction time led to different modifications in the biomechanical properties of the BNS. All groups, except GP 0.05% (6 h), displayed significantly higher values of Young's modulus than NGP ($p<0.05$, Supplementary Table S2). Interestingly, GP 0.2% at 24 h showed the highest values for the Young's modulus, followed by GP 0.1% at 12 h and GP 0.05% at 72 h. Surprisingly, increasing GP concentration did not always result in the highest values of Young's modulus, neither increasing the GP reaction time. Actually, it was observed that the same or even higher Young's modulus values could be achieved with lower concentrations and longer reaction times. The diverse effects of different GP concentrations and reaction times on the biomechanical properties of BNS crosslinked with GP indicated a non-linear response and highlighted that an optimization of both is necessary for each material to match the required properties.

3.3. Ex vivo biocompatibility of genipin-crosslinked bioartificial nerve substitutes

The potential biocompatibility effects of GP crosslinked BNS were assessed by using a double approach on macrophages: by evaluating the cytotoxic effects using the LIVE/DEAD method and by assessing the cell metabolic activity using the WST-1 method (Fig. 3).

First, microscopic examination of LIVE/DEAD analysis (Fig. 3A) revealed no adverse effects on macrophages exposed to GP crosslinked BNS. Representative images demonstrated that neither the increasing GP concentration nor the reaction time had any detrimental impact on cell viability, as there were no detectable dead cells in the cultures (Fig. 3A).

Metabolic and proliferation activity changes influenced by GP crosslinked BNS were shown in Fig. 3B. In general, overall WST-1 results indicated minimal effects on macrophage metabolic activity. Regarding global groups, according to GP concentration or reaction time, it was found that only at the highest GP concentration (0.2%) and the longest GP reaction time (72 h) did show a significant reduction of the metabolic activity as compared to the control group (CTR+), with values reduced to 98.58% ($p = 0.01$) and 98.74% ($p = 0.022$), respectively (Supplementary Table S2). Additionally, the metabolic activity showed a negative correlation between both the GP concentration ($r=-0.13$, $p<0.05$) and the crosslinking reaction time ($r=-0.18$, $p<0.05$). Finally, further examination of specific sample groups revealed that lower GP concentrations and shorter reaction times had negligible effects on macrophage metabolic activity. Only GP 0.2% at 12 h, 24 h, and 72 h displayed statistically significant lower values than CTR+ group ($p<0.05$, Supplementary Table S2).

Then, fibroblasts human cells were used to assess GP crosslinked BNS biocompatibility by evaluating the cytotoxic effects using the LIVE/DEAD method. The microscopic evaluation showed no adverse effect on fibroblast viability after 3 or 7 days of direct contact with the highest GP crosslinked BNS (Supplementary figure S2).

3.4. Immunomodulatory effects of genipin-crosslinked bioartificial nerve substitutes on macrophages

The immunomodulatory impact of GP crosslinked BNS on macrophage cell cultures was assessed in a two-step study. First, the phenotypic modulation of macrophages by the expression of pro-inflammatory or pro-regenerative clusters of differentiation markers (CD86 and CD163 respectively) was studied (Fig. 4A, B and C); then, the profile of cytokine release was determined (Fig. 4D and E).

Regarding the clusters of differentiation -CD- markers, the results revealed that GP crosslinking induced a reduction in undifferentiated macrophages (M0) and an increase in pro-regenerative macrophages (M2) in a time and concentration dependent manner. Actually,

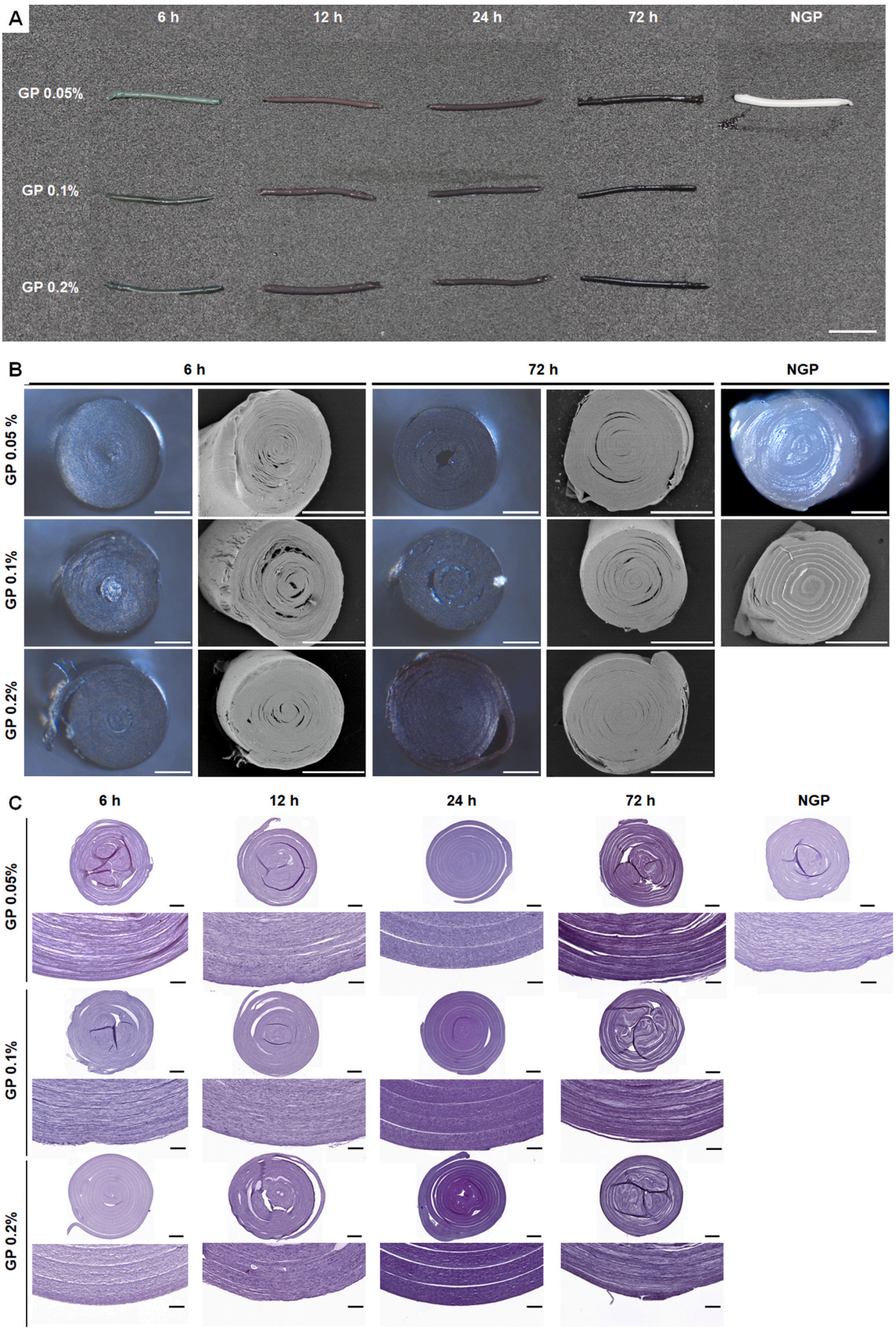

Fig. 1. Macroscopical and microscopical analysis of genipin-crosslinked (GP) bioartificial nerve substitutes (BNS). A shows macroscopical images of longitudinally oriented BNS whereas images in B shows representative macroscopic and scanning electron microscopy cross-sectioned BNS images. Images in C shows haematoxylin-eosin (H&E) stained cross-sections of the different BNS. Not crosslinked BNS were used as control (NGP). Scales bar: A: 1 mm; B: 500 μm C: 200 μm and 50 μm for insets.

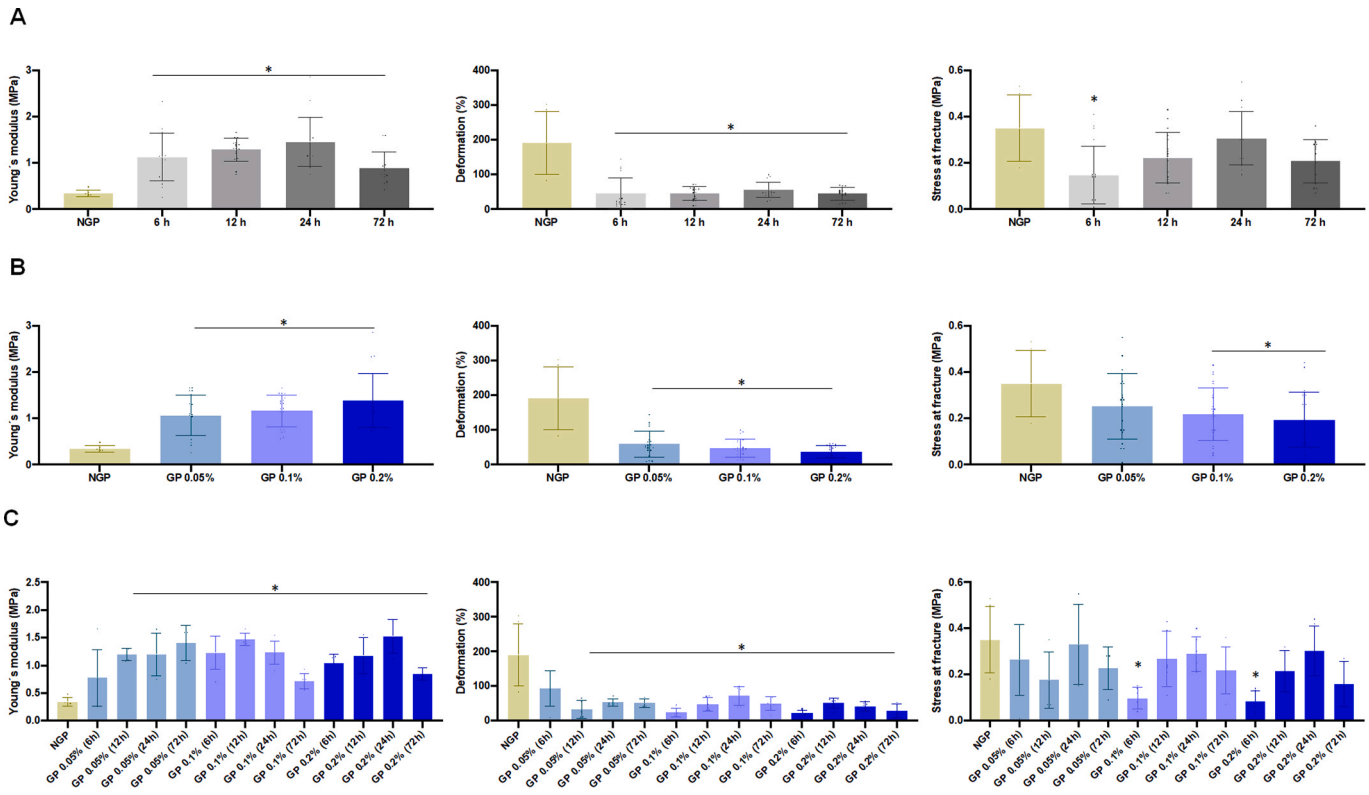

Fig. 2. Biomechanical characterization of genipin-crosslinked (GP) bioartificial nerve substitutes (BNS). Traction analysis results of Young's modulus, traction deformation, and stress at fracture of BNS based on global groups regarding GP reaction time (A) or GP concentration (B) and based on specific sample groups (C). Not crosslinked BNS were used as control (NGP). Only statistically significant differences with NGP control group are included and marked as "*", all other comparisons are included in supplementary table S2.

undifferentiated double negative macrophages showed a negative correlation with both the GP concentration and the reaction time ($r=-0.45$, $p<0.05$ and $r=-0.42$, $p<0.05$ respectively), whereas CD163-positive M2 cells displayed a positive correlation with both the GP concentration and the reaction time ($r=0.45$, $p<0.05$ and $r=0.16$, $p<0.05$, respectively).

In the same line, GP crosslinking did not evoke a pro-inflammatory phenotype change in culture macrophages. In fact, all GP crosslinked BNS displayed significant differences with the M1 control group ($p<0.05$, Supplementary Table S2) and neither the GP reaction time, nor the concentration showed any significant increase in CD86 positive cells as compared to the undifferentiated M0 control group. A significant reduction of GP reaction time was observed at 6 h as compared to the undifferentiated M0 control group (Fig. 4A and B).

The reduction in undifferentiated macrophages was statistically significant at all GP reaction times and from a GP concentration of 0.1% ($p<0.05$, Fig. 4A and B and Supplementary Table S2), which was associated with an increase of CD163 positive cells from 6 h GP reaction time and 0.1% GP concentration, as compared to the M0 control group ($p<0.05$, Supplementary Table S2). Interestingly, GP modification of BNS resulted in a significant increase in CD163 pro-regenerative cells as compared to NGP BNS in all GP reaction times and concentrations (Fig. 4A and B, $p<0.05$, Supplementary Table S2).

Additionally, we analysed if the biomechanical properties could influence macrophage phenotype, and we found that the percentage of macrophage cells showing positive CD86 or CD163 expression was not correlated with the Young's modulus ($p>0.05$ for the test of Kendall for both markers).

Further analysis of specific sample groups showed that the CD163-positive cell population started to increase significantly at GP 0.05% 72 h, as from this point on, significant differences between the control M0 and all the experimental groups were found (Fig. 4C, p values in Supplementary Table S2).

Finally, we assess the profile of cytokine release on cells incubated in the presence of BNS crosslinked with the highest concentrations of GP. Results (Fig. 5) first showed that the profile of cytokine release was mainly pro-inflammatory in the M1 control group, with an increase of CS/C5a, G-CSF, IL-3, IL-17, IL-23, and TNFα, whereas the M0 control group tended to display a pro-regenerative and anti-inflammatory profile with increased expression of IL-2, IL-10, IL-13, and SDF-1, as expected. For the NGP and BNS groups, the profile of cytokines expression is shown in Fig. 5. When these results were compared, and samples were classified based on their profile for these cytokines using hierarchical clustering, we found that BNS crosslinked with 0.2% GP clustered together with the M0 control group, whereas NGP formed an independent clustering branch and, finally, the M1 control group was found to be the most distant group.

4. Discussion

In this study, we aimed to evaluate, for the first time, the effect of GP crosslinking in a time and concentration-dependent manner on BNS based on FA hydrogels. In this line, the biomechanical properties under tensile test and anti-inflammatory properties were determined *ex vivo* for potential tissue regeneration applications.

Previous research already demonstrated the efficacy of FA-based BNS in peripheral nerve repair *in vitro* and in the rat sciatic nerve injury model [13,14]. However, despite employing nanostructured techniques to enhance the mechanical properties of FA hydrogels, they still lacked the appropriate mechanical properties for certain applications [13,14,37]. To address this limitation, we investigated the mechanical and immunological effect of the interaction between GP and fibrin-agarose biomaterials in the BNS.

GP, a natural iridoid glycoside derived from the fruit of *Gardenia jasminoides*, has been commonly used to enhance the biomechanical

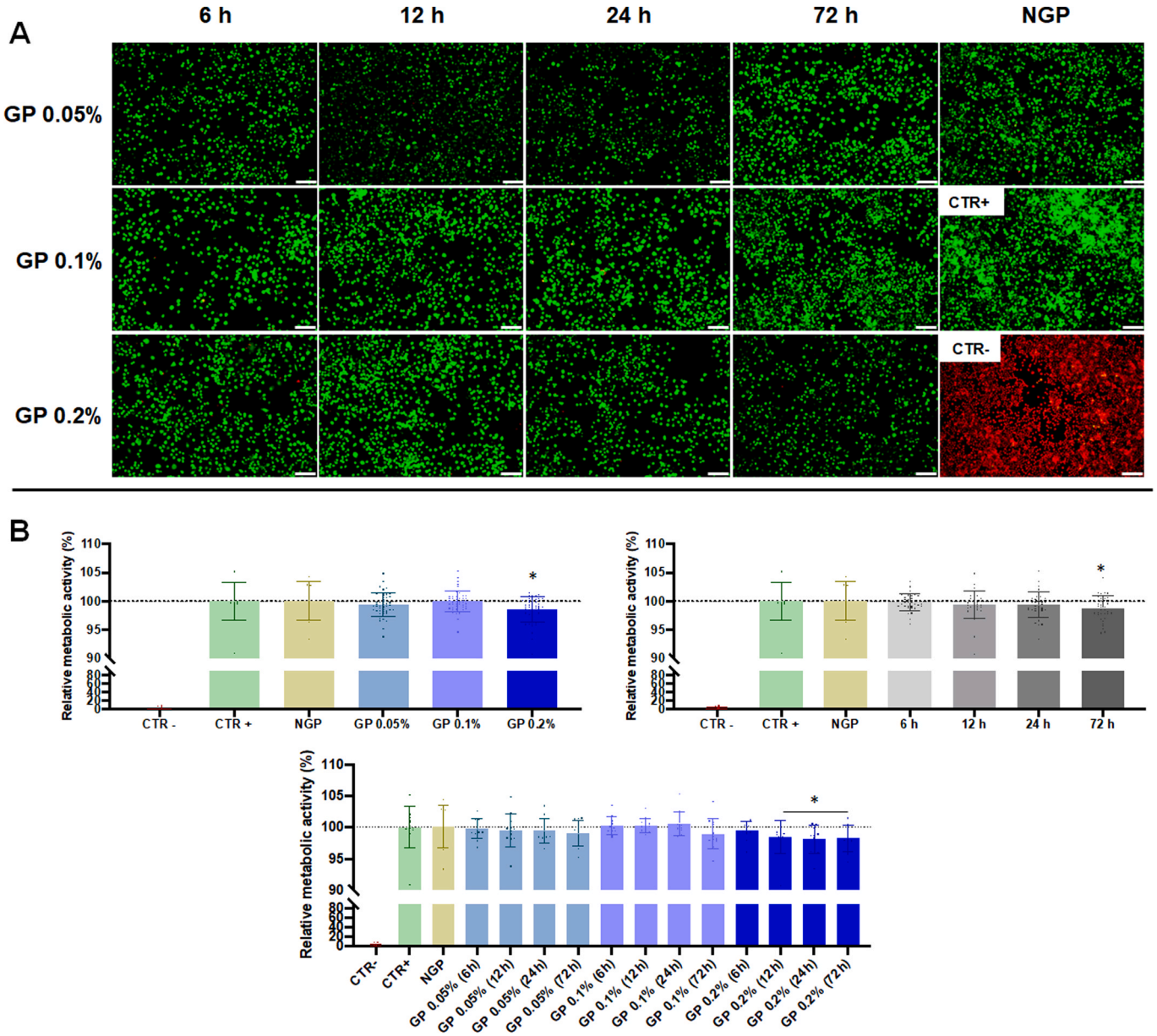

Fig. 3. *Ex vivo* biocompatibility assessment of genipin-crosslinked (GP) bioartificial nerve substitutes (BNS) on macrophage cultures. Microscopic images of LIVE/DEAD analysis (A) and WST-1 results (B) of global groups regarding GP concentration, GP reaction time and of specific sample groups results. WST-1 were normalized with the negative and positive control group considered as 0% and 100% metabolic activity respectively. Only statistically significant differences with CTR+ control group are included and marked as "*", all other comparisons are included in supplementary table S2. Scale bar: 100 μm.

properties of biomaterials in tissue engineering, including nerve guidance conduits and decellularized matrices [21,38,39], along with other FA-based tissues and organs such as the sclera, cornea and skin [24,25]. Previous studies demonstrated the interaction of GP with fibrin and agarose separately, which is based on the generation of covalent bonds with free primary amines in fibrin and a fraction of amino acids in agarose [40,41]. These interactions led to enhanced biomechanical properties, reduced degradation, and improved stability in both materials indicated by a distinct dark blue color [40,41]. Our study showed that GP crosslinked BNS displayed a homogenously dark blue color, which is time and concentration dependent, with the presence of uniformly organized and interconnected horizontally oriented layers of fibers. These results confirm that GP efficiently diffused through the nanostructured FA scaffolds and reacted homogeneously, yielding stable and robust BNS as shown in the macroscopic and microscopic characterization results.

From a structural and biomechanical perspective, it is imperative for tissue engineering substitutes to possess sufficient resistance, flexibility, and elasticity to facilitate easy handling during surgical implantation [3,7,21]. In this sense, GP crosslinked BNS demonstrated improved biomechanical properties from a concentration of 0.05% and a reaction time of 6 h onwards, which are vital for their potential clinical applications [24]. GP-induced improvements in biomechanical resistance were dependent on both GP reaction time and concentration. Interestingly, Young's modulus initially increased up to 24 h of GP reaction and then decreased at longer reaction times, suggesting the importance of an optimal crosslinking time. Similarly, increasing GP concentrations positively influenced Young's modulus, leading to stiffer BNS, but with reduced deformation properties, as evidenced by decreased strain at fracture and percentage of deformation. In general, BNS displayed different results of mechanical strength and deformability based on time and concentration, which underlines the need of optimizing both

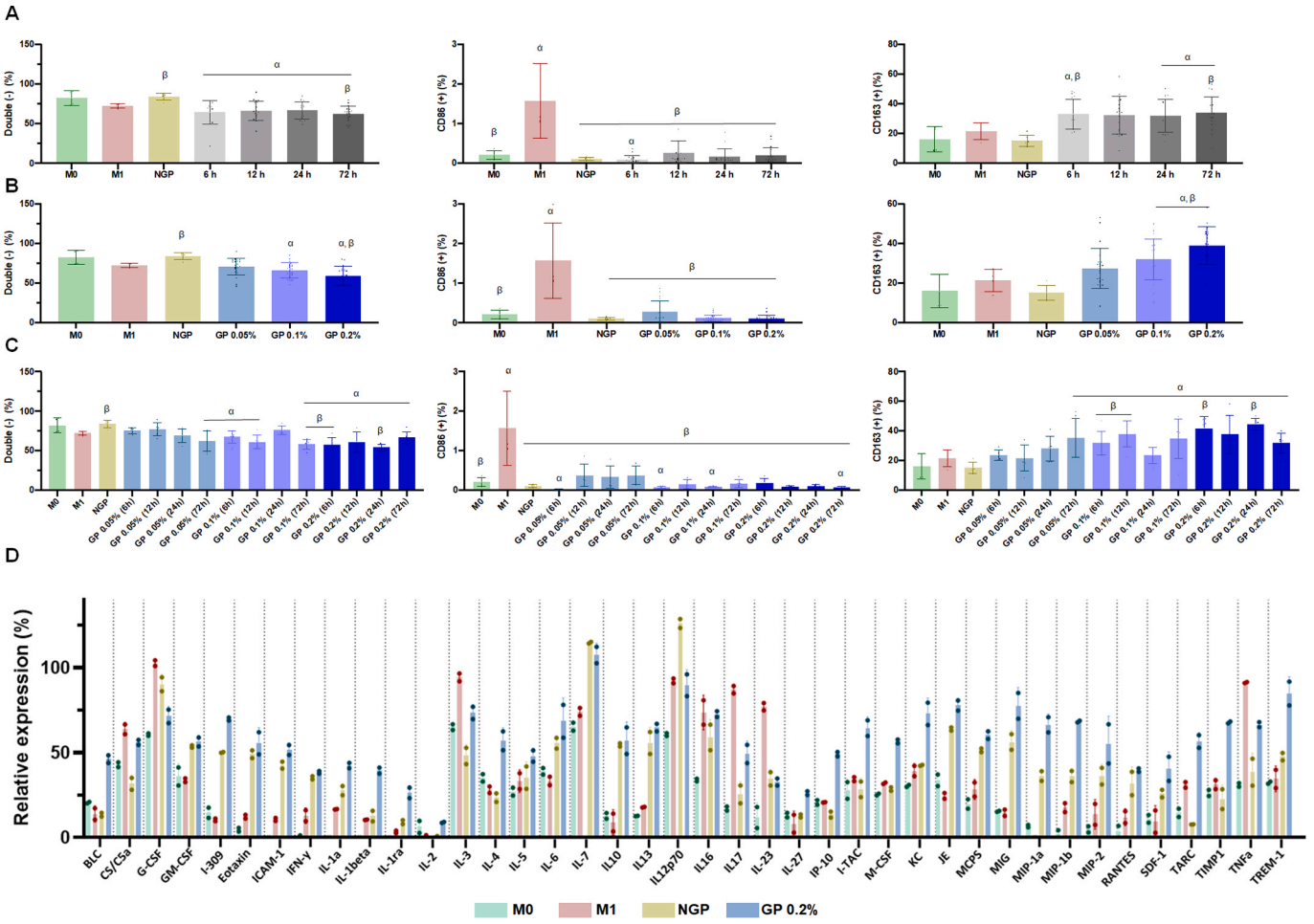

Fig. 4. Immunomodulatory effects of genipin-crosslinked (GP) bioartificial nerve substitutes (BNS) Phenotypic modulation of macrophages assessed by clusters of differentiation markers (CD86 and CD163) of global groups regarding GP reaction time (A), GP concentration (B) and of specific sample groups results (C) represented as percentage of cells. Relative cytokines expression released by macrophages in response to GP crosslinked BNS (D). Only statistically significant differences with M0 and M1 control groups are included and marked as "α" and "β" respectively, all other comparisons are included in supplementary table S2.

parameters to achieve the desired mechanical properties. Prolonged GP reaction times or concentrations beyond the optimal range may lead to a decrease in biomechanical properties. Concentration and time are crucial parameters that need to be tightly controlled to balance mechanical strength and deformability of bioartificial tissues [24], especially in the case of tubular organs, such as the human nerve or the urethra.

While GP is generally considered a low-toxicity crosslinking agent [42,43], some studies have reported dose-dependent toxic effects when directly exposing cells to GP in tissue engineering applications [24,44,45]. Our biocompatibility analysis of GP crosslinked BNS using macrophage and human cell cultures confirmed no cytotoxic effects by LIVE/DEAD, and a minimal reduction of metabolic activity by WST-1. Although WST-1 confirmed an indirect correlation between GP concentration and cell metabolic activity, only minimal detrimental effects were found using 0.2% GP for 12, 24 and 72 h, reducing cell activity by only 2%, as compared to the CTR+ group. In the same line, the metabolic activity of macrophages was not affected in the GP 0.05% and GP 0.1% groups. These results are in accordance with previous studies confirming the absence of cytotoxic effects in GP-crosslinked scaffolds [43,46].

In order to evaluate *ex vivo* the possible future host response of GP crosslinked BNS, we evaluated its immunomodulatory effects in a macrophage culture, and we found that crosslinked BNS exerted, in general, a pro-regenerative profile on the cultured cells. Our study demonstrated that all experimental groups showed significantly lower percentages of pro-inflammatory M1 phenotypes, and from GP 0.05% 72 h onwards, all the groups showed high M2 phenotype cell populations. These results proved that GP-crosslinked BNS effectively directed macrophage polarization from a pro-inflammatory (M1) phenotype towards a pro-regenerative (M2) phenotype. Strikingly, the increase in M2 macrophages was found to be both, time and concentration dependent. These results agree with the cytokines release profile results, as GP-crosslinked BNS promoted the release of pro-regenerative cytokines, such as IL-2, IL-10, IL-13, and SDF-1, while reducing the expression of pro-inflammatory cytokines, like CS/C5a, G-CSF, IL-3, IL-17, IL-23, and TNFα. This suggests that GP may not only direct macrophage polarization but also facilitate the secretion of cytokines that support tissue repair and regeneration. All these findings are supported by previous research which demonstrated that crosslinking techniques hinder immunogenic binding sites, leading to delayed exposure of active structural domains [47]. This reaction also aims to extend the degradation and maximize tissue remodelling effects while minimizing inflammatory responses by loading cells [47,48]. In addition to the chemical signals, macrophage modulation could also be influenced by the biophysical cues of the material [49–51]. Published literature demonstrated that macrophages are able to adapt their polarization, function and migration mode in response to the stiffness of the underlying substrate [49,51]. Although we found that the mechanical strength was impacted by the GP crosslinking reaction, and the highest concentrations of GP increased the Young's Modulus, we found that the correlation of this parameter with macrophage phenotype was

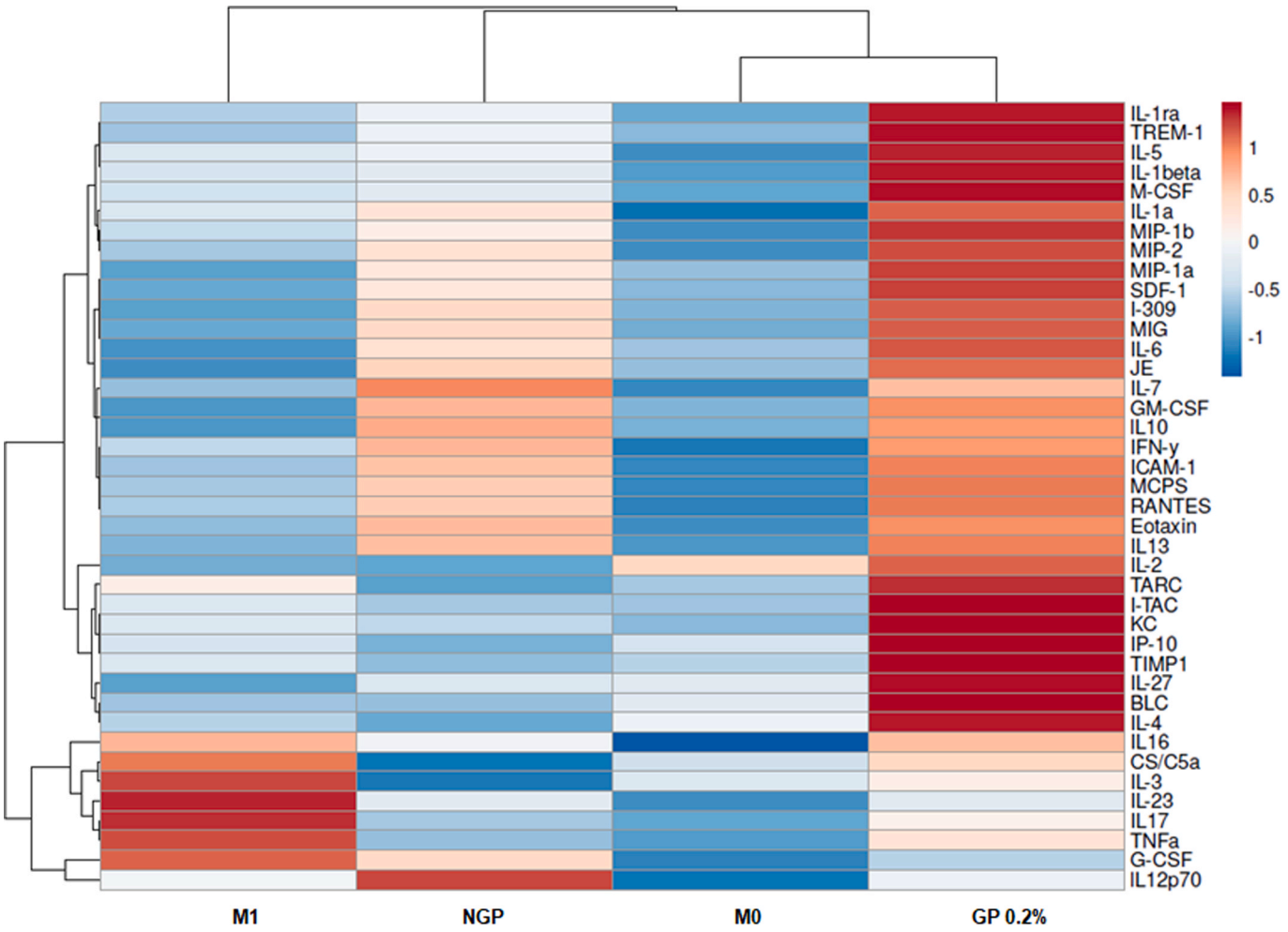

Fig. 5. Hierarchical clustering classification of genipin-crosslinked (GP) bioartificial nerve substitutes (BNS) based on the global released cytokine profile of macrophages. Heat map and dendogram of cluster analysis on the inflammatory response of RAW cells, tested trough cytokines and chemokines expression (Proteome ProfilerTM cytokine array).

non-significant. However, in this work, macrophage culture strategy involved indirect contact with our BNS, which allowed us to study macrophage differentiation through soluble chemical cues released by the BNS rather than by a real physical nor topographic influence of the material. Future studies should investigate the specific impact of scaffold mechanical strength on macrophage phenotype under direct cell culture conditions. Additionally, our results could be also explained by the previously demonstrated polarization of macrophages to the pro-regenerative M2 subtype via activation of the pSTAT6-PPAR-gamma pathway by GP [27,28]. The ability of GP-crosslinked BNS to induce M2 polarization and promote regenerative responses are normally associated with tissue repair, collagen deposition, and extracellular matrix production, making them essential for successful nerve regeneration [28,39,52]. However, future analyses should also be performed after longer incubation times, for a more precise understanding of macrophage differentiation patterns and adaptation, not only at short-terms, but also at the long-term.

In this study, we utilized a macrophage cell line for the initial assessment of the immunomodulatory effects of our BNS, and a human cell culture to test scaffolds biocompatibility. Future research should evaluate the influence of the different biomaterials on other types of cells, including neural-like cell lines in order to determine the specific effects of these scaffolds applied to nerve regeneration, such as neurite outgrowth and myelination. In any case, the promising outcomes observed in our *ex vivo* characterization strongly advocate for further *in vivo* investigations to assess the potential of GP-crosslinked BNS in nerve repair applications. As we progress towards clinical translation, it is essential to adhere to the principles of reduction, refinement, and replacement of animal experiments by conducting a thorough *ex vivo* characterization prior to animal testing. In this *ex vivo* study, we were able to optimize GP crosslinking time and concentration and we can minimize the need for animal experiments which ensures a responsible, ethical and efficient pathway for the development of advanced biomaterials for nerve repair.

In conclusion, our study presents the first comprehensively evaluation of GP crosslinking reaction in FA-based hydrogels, considering its time and dose-dependent effects, and highlighting its potential as a powerful tool for nerve repair applications, as well as other tubular organs such as the human urethra. Our GP crosslinked BNS displayed a stable cylindrical shape with increased biomechanical properties while reducing immunogenicity and promoting pro-regenerative macrophage shift. The combination of all these effects makes GP a useful crosslinking tool in tissue engineering after optimizing both time and concentration for each intended application. Here, GP generated new BNS and provides a strong foundation for further exploration in *in vivo* models.

CRediT authorship contribution statement

Jone Berasain: Writing – original draft, Visualization, Validation, Investigation, Formal analysis, Data curation. **Paula Ávila-Fernández:** Validation, Investigation. **Rocío Cárdenas-Pérez:** Validation, Investigation. **Antoni Ignasi Cànaves-Llabrés:** Software. **Miguel Etayo-**

Escanilla: Validation, Software. **Miguel Alaminos:** Writing – review & editing, Formal analysis. **Víctor Carriel:** Writing – review & editing, Funding acquisition, Formal analysis. **Óscar Darío García García:** Writing – review & editing, Visualization, Methodology, Funding acquisition, Formal analysis, Conceptualization. **Jesús Chato-Astrain:** Writing – original draft, Visualization, Supervision, Methodology, Funding acquisition, Formal analysis, Conceptualization. **Fernando Campos:** Writing – review & editing, Visualization, Supervision, Methodology, Funding acquisition, Formal analysis, Conceptualization.

Declaration of Competing Interest

The authors declare that they have no known competing financial interests or personal relationships that could have appeared to influence the work reported in this paper.

Acknowledgements

This work was supported by the Tissue Engineering Research Group (CTS-115), the Spanish "Plan Nacional de Investigación Científica, Desarrollo e Innovación Tecnológica" (I+D+i) of the Ministry of Science and Innovation of Spain (Instituto de Salud Carlos III), Grants FIS PI20/00318, PI23/00337 and PI22/00059, co-financed by FEDER funds (European Union); Grant CPP2021–009070 by the "Proyectos de colaboración público-privada, Plan de Investigación Científica, Técnica y de innovación 2021–2023, Ministerio de Ciencia e Innovación, Unión Europea, Agencia Estatal de Investigación, España. Also supported by Grant PPJIA2022-19 "Ayudas del plan propio UGR 2022, Plan propio de investigación y transferencia, Universidad de Granada, España".

Appendix A. Supporting information

Supplementary data associated with this article can be found in the online version at doi:10.1016/j.biopha.2024.116449.

References

[1] D. Cinteza, I. Persinaru, B.M. Maciuceanu Zarnescu, D. Ionescu, I. Lascar, Peripheral nerve regeneration - an appraisal of the current treatment options, Maedica (Bucur) 10 (1) (2015) 65–68.
[2] G. Ciardelli, V. Chiono, Materials for peripheral nerve regeneration, Macromol. Biosci. 6 (1) (2006) 13–26.
[3] V. Carriel, M. Alaminos, I. Garzon, A. Campos, M. Cornelissen, Tissue engineering of the peripheral nervous system, Expert Rev. Neurother. 14 (3) (2014) 301–318.
[4] A. Faroni, S.A. Mobasseri, P.J. Kingham, A.J. Reid, Peripheral nerve regeneration: experimental strategies and future perspectives, Adv. Drug Deliv. Rev. 82-83 (2015) 160–167.
[5] L. Kong, X. Gao, Y. Qian, W. Sun, Z. You, C. Fan, Biomechanical microenvironment in peripheral nerve regeneration: from pathophysiological understanding to tissue engineering development, Theranostics 12 (11) (2022) 4993–5014.
[6] Y. Hu, Y. Wu, Z. Gou, J. Tao, J. Zhang, Q. Liu, T. Kang, S. Jiang, S. Huang, J. He, S. Chen, Y. Du, M. Gou, 3D-engineering of cellularized conduits for peripheral nerve regeneration, Sci. Rep. 6 (2016) 32184.
[7] O.D. Garcia-Garcia, M. El Soury, F. Campos, D. Sanchez-Porras, S. Geuna, M. Alaminos, G. Gambarotta, J. Chato-Astrain, S. Raimondo, V. Carriel, Comprehensive ex vivo and in vivo preclinical evaluation of novel chemo enzymatic decellularized peripheral nerve allografts, Front Bioeng. Biotechnol. 11 (2023) 1162684.
[8] J. Chato-Astrain, O. Roda, D. Sanchez-Porras, E. Miralles, M. Alaminos, F. Campos, O.D. Garcia-Garcia, V. Carriel, Peripheral nerve regeneration through nerve conduits evokes differential expression of growth-associated protein-43 in the spinal cord, Neural Regen. Res 18 (8) (2023) 1852–1856.
[9] S. Kehoe, X.F. Zhang, D. Boyd, FDA approved guidance conduits and wraps for peripheral nerve injury: a review of materials and efficacy, Injury 43 (5) (2012) 553–572.
[10] C. Gonzalez-Gallardo, J. Martinez-Atienza, B. Mataix, J.I. Munoz-Avila, J. Daniel Martinez-Rodriguez, S. Medialdea, A. Ruiz-Garcia, A. Lizana-Moreno, S. Arias-Santiago, M. de la Rosa-Fraile, I. Garzon, A. Campos, N. Cuende, M. Alaminos, M. Gonzalez-Andrades, R. Mata, Successful restoration of corneal surface integrity with a tissue-engineered allogeneic implant in severe keratitis patients, Biomed. Pharm. 162 (2023) 114612.
[11] J.J. Egea-Guerrero, G. Carmona, E. Correa, R. Mata, S. Arias-Santiago, M. Alaminos, P. Gacto, N. Cuende, Transplant of tissue-engineered artificial autologous human skin in andalusia: an example of coordination and institutional collaboration, Transpl. Proc. 51 (9) (2019) 3047–3050.
[12] V. Carriel, J. Garrido-Gomez, P. Hernandez-Cortes, I. Garzon, S. Garcia-Garcia, J. A. Saez-Moreno, M. Del Carmen Sanchez-Quevedo, A. Campos, M. Alaminos, Combination of fibrin-agarose hydrogels and adipose-derived mesenchymal stem cells for peripheral nerve regeneration, J. Neural Eng. 10 (2) (2013) 026022.
[13] V. Carriel, G. Scionti, F. Campos, O. Roda, B. Castro, M. Cornelissen, I. Garzon, M. Alaminos, In vitro characterization of a nanostructured fibrin agarose bio-artificial nerve substitute, J. Tissue Eng. Regen. Med. 11 (5) (2017) 1412–1426.
[14] J. Chato-Astrain, F. Campos, O. Roda, E. Miralles, D. Durand-Herrera, J.A. Saez-Moreno, S. Garcia-Garcia, M. Alaminos, A. Campos, V. Carriel, In vivo evaluation of nanostructured fibrin-agarose hydrogels with mesenchymal stem cells for peripheral nerve repair, Front Cell Neurosci. 12 (2018) 501.
[15] N. Reddy, R. Reddy, Q. Jiang, Crosslinking biopolymers for biomedical applications, Trends Biotechnol. 33 (6) (2015) 362–369.
[16] F. Ruini, C. Tonda-Turo, V. Chiono, G. Ciardelli, Chitosan membranes for tissue engineering: comparison of different crosslinkers, Biomed. Mater. 10 (6) (2015) 065002.
[17] J. Robinson, T. Russell, Z. Xu, Y. Yun, Mechanically tunable extracellular matrix of genipin crosslinked collagen and its effect on endothelial function, Appl. Sci. (Basel) 12 (5) (2022).
[18] B.T. Wonski, B. Fisher, M.T. Lam, Hydrogel coating optimization to augment engineered soft tissue mechanics in tissue-engineered blood vessels, Bioeng. (Basel) 10 (7) (2023).
[19] G. Gorczyca, R. Tylingo, P. Szweda, E. Augustin, M. Sadowska, S. Milewski, Preparation and characterization of genipin cross-linked porous chitosan-collagen-gelatin scaffolds using chitosan-CO2 solution, Carbohydr. Polym. 102 (2014) 901–911.
[20] E. Sharifi, S. Yousefiasl, N. Laderian, N. Rabiee, P. Makvandi, S. Pourmotabed, M. Ashrafizadeh, F. Familsattarian, W. Fang, Cell-loaded genipin cross-linked collagen/gelatin skin substitute adorned with zinc-doped bioactive glass-ceramic for cutaneous wound regeneration, Int. J. Biol. Macromol. (2023) 125898.
[21] O.D. Garcia-Garcia, M. El Soury, D. Gonzalez-Quevedo, D. Sanchez-Porras, J. Chato-Astrain, F. Campos, V. Carriel, Histological, biomechanical, and biological properties of genipin-crosslinked decellularized peripheral nerves, Int. J. Mol. Sci. 22 (2) (2021).
[22] Y. Tang, W. Song, J. Qiao, B. Rong, Y. Wu, X. Yan, A study of corneal structure and biomechanical properties after collagen crosslinking with genipin in rabbit corneas, Mol. Vis. 25 (2019) 574–582.
[23] T. Jiang, X.J. Ren, J.L. Tang, H. Yin, K.J. Wang, C.L. Zhou, Preparation and characterization of genipin-crosslinked rat acellular spinal cord scaffolds, Mater. Sci. Eng. C Mater. Biol. Appl. 33 (6) (2013) 3514–3521.
[24] F. Campos, A.B. Bonhome-Espinosa, G. Vizcaino, I.A. Rodriguez, D. Duran-Herrera, M.T. Lopez-Lopez, I. Sanchez-Montesinos, M. Alaminos, M.C. Sanchez-Quevedo, V. Carriel, Generation of genipin cross-linked fibrin-agarose hydrogel tissue-like models for tissue engineering applications, Biomed. Mater. 13 (2) (2018) 025021.
[25] V. Carriel, G. Vizcaino-Lopez, J. Chato-Astrain, D. Durand-Herrera, M. Alaminos, A. Campos, I. Sanchez-Montesinos, F. Campos, Scleral surgical repair through the use of nanostructured fibrin/agarose-based films in rabbits, Exp. Eye Res 186 (2019) 107717.
[26] D. Gonzalez-Quevedo, M. Diaz-Ramos, J. Chato-Astrain, D. Sanchez-Porras, I. Tamimi, A. Campos, F. Campos, V. Carriel, Improving the regenerative microenvironment during tendon healing by using nanostructured fibrin/agarose-based hydrogels in a rat Achilles tendon injury model, Bone Jt. J. 102-B (8) (2020) 1095–1106.
[27] I. Isali, P. McClellan, T.R. Wong, S. Cingireddi, M. Jain, J.M. Anderson, A. Hijaz, O. Akkus, In vivo delivery of M0, M1, and M2 macrophage subtypes via genipin-cross-linked collagen biotextile, Tissue Eng. Part A 28 (15-16) (2022) 672–684.
[28] I. Isali, P. McClellan, E. Shankar, S. Gupta, M. Jain, J.M. Anderson, A. Hijaz, O. Akkus, Genipin guides and sustains the polarization of macrophages to the pro-regenerative M2 subtype via activation of the pSTAT6-PPAR-gamma pathway, Acta Biomater. 131 (2021) 198–210.
[29] C. Blanco-Elices, C. Morales-Alvarez, J. Chato-Astrain, C. Gonzalez-Gallardo, P. Avila-Fernandez, F. Campos, R. Carmona, M.A. Martin-Piedra, I. Garzon, M. Alaminos, Development of stromal differentiation patterns in heterotypical models of artificial corneas generated by tissue engineering, Front Bioeng. Biotechnol. 11 (2023) 1124995.
[30] O. Ortiz-Arrabal, A. Irastorza-Lorenzo, F. Campos, M.A. Martin-Piedra, V. Carriel, I. Garzon, P. Avila-Fernandez, M.J. de Frutos, E. Esteban, J. Fernandez, A. Janer, A. Campos, J. Chato-Astrain, M. Alaminos, Fibrin and marine-derived agaroses for the generation of human bioartificial tissues: an ex vivo and in vivo study, Mar. Drugs 21 (3) (2023).
[31] M. Ibanez-Cortes, M.A. Martin-Piedra, C. Blanco-Elices, O.D. Garcia-Garcia, A. Espana-Lopez, R. Fernandez-Valades, M.D.C. Sanchez-Quevedo, M. Alaminos, J. Chato-Astrain, I. Garzon, Histological characterization of the human masticatory oral mucosa. A histochemical and immunohistochemical study, Microsc. Res. Tech. 86 (12) (2023) 1712–1724.
[32] E.R. Fischer, B.T. Hansen, V. Nair, F.H. Hoyt, D.W. Dorward, Scanning electron microscopy, Curr. Protoc. Microbiol. Chapter 2 (2012). Unit 2B 2.
[33] A.M. Ionescu, J. Chato-Astrain, J.C. Cardona Perez, F. Campos, M. Perez Gomez, M. Alaminos, I. Garzon Bello, Evaluation of the optical and biomechanical properties of bioengineered human skin generated with fibrin-agarose biomaterials, J. Biomed. Opt. 25 (5) (2020) 1–16.
[34] M. Cutolo, R. Campitiello, E. Gotelli, S. Soldano, The role of M1/M2 macrophage polarization in rheumatoid arthritis synovitis, Front Immunol. 13 (2022) 867260.
[35] O. Cases-Perera, C. Blanco-Elices, J. Chato-Astrain, C. Miranda-Fernandez, F. Campos, P.V. Crespo, I. Sanchez-Montesinos, M. Alaminos, M.A. Martin-Piedra,

I. Garzon, Development of secretome-based strategies to improve cell culture protocols in tissue engineering, Sci. Rep. 12 (1) (2022) 10003.
[36] T. Metsalu, J. Vilo, ClustVis: a web tool for visualizing clustering of multivariate data using Principal Component Analysis and heatmap, Nucleic Acids Res. 43 (W1) (2015) W566–W570.
[37] F. Campos, A.B. Bonhome-Espinosa, L. Garcia-Martinez, J.D. Duran, M.T. Lopez-Lopez, M. Alaminos, M.C. Sanchez-Quevedo, V. Carriel, Ex vivo characterization of a novel tissue-like cross-linked fibrin-agarose hydrogel for tissue engineering applications, Biomed. Mater. 11 (5) (2016) 055004.
[38] K. Vyborny, J. Vallova, Z. Koci, K. Kekulova, K. Jirakova, P. Jendelova, J. Hodan, S. Kubinova, Genipin and EDC crosslinking of extracellular matrix hydrogel derived from human umbilical cord for neural tissue repair, Sci. Rep. 9 (1) (2019) 10674.
[39] Z. Koci, R. Sridharan, A.J. Hibbitts, S.L. Kneafsey, C.J. Kearney, F.J. O'Brien, The use of genipin as an effective, biocompatible, anti-inflammatory cross-linking method for nerve guidance conduits, Adv. Biosyst. 4 (3) (2020).
[40] R. Meena, K. Prasad, A.K. Siddhanta, Preparation of genipin-fixed agarose hydrogel, J. Appl. Polym. Sci. 104 (1) (2007) 290–296.
[41] C. Ninh, A. Iftikhar, M. Cramer, C.J. Bettinger, Diffusion-Reaction Models of Genipin Incorporation into Fibrin Networks, J. Mater. Chem. B 3 (22) (2015) 4607–4615.
[42] Y. Zhang, Q.S. Wang, K. Yan, Y. Qi, G.F. Wang, Y.L. Cui, Preparation, characterization, and evaluation of genipin crosslinked chitosan/gelatin three-dimensional scaffolds for liver tissue engineering applications, J. Biomed. Mater. Res A 104 (8) (2016) 1863–1870.
[43] Y. Xi-xun, L. Fei, X. Yuan-ting, W. Chang-xiu, In vitro study in the endothelial cell compatibility and endothelialization of genipin-crosslinked biological tissues for tissue-engineered vascular scaffolds, J. Mater. Sci. Mater. Med. 21 (2) (2010) 777–785.
[44] G. Fessel, J. Cadby, S. Wunderli, R. van Weeren, J.G. Snedeker, Dose- and time-dependent effects of genipin crosslinking on cell viability and tissue mechanics - toward clinical application for tendon repair, Acta Biomater. 10 (5) (2014) 1897–1906.
[45] F. Mwale, M. Iordanova, C.N. Demers, T. Steffen, P. Roughley, J. Antoniou, Biological evaluation of chitosan salts cross-linked to genipin as a cell scaffold for disk tissue engineering, Tissue Eng. 11 (1-2) (2005) 130–140.
[46] T. Suchy, M. Supova, P. Sauerova, M. Verdanova, Z. Sucharda, S. Ryglova, M. Zaloudkova, R. Sedlacek, M.H. Kalbacova, The effects of different cross-linking conditions on collagen-based nanocomposite scaffolds-an in vitro evaluation using mesenchymal stem cells, Biomed. Mater. 10 (6) (2015) 065008.
[47] J. Long, Z. Qin, G. Chen, B. Song, Z. Zhang, Decellularized extracellular matrix (d-ECM): the key role of the inflammatory process in pre-regeneration after implantation, Biomater. Sci. 11 (4) (2023) 1215–1235.
[48] M. Kasravi, A. Ahmadi, A. Babajani, R. Mazloomnejad, M.R. Hatamnejad, S. Shariatzadeh, S. Bahrami, H. Niknejad, Immunogenicity of decellularized extracellular matrix scaffolds: a bottleneck in tissue engineering and regenerative medicine, Biomater. Res 27 (1) (2023) 10.
[49] Z. Liu, J. Zhu, Z. Li, H. Liu, C. Fu, Biomaterial scaffolds regulate macrophage activity to accelerate bone regeneration, Front Bioeng. Biotechnol. 11 (2023) 1140393.
[50] B. Zhang, M. Galluzzi, G. Zhou, H. Yu, A study of macrophage mechanical properties and functional modulation based on the Young's modulus of PLGA-PEG fibers, Biomater. Sci. 11 (1) (2022) 153–161.
[51] R. Sridharan, B. Cavanagh, A.R. Cameron, D.J. Kelly, F.J. O'Brien, Material stiffness influences the polarization state, function and migration mode of macrophages, Acta Biomater. 89 (2019) 47–59.
[52] R. Sridharan, E.J. Ryan, C.J. Kearney, D.J. Kelly, F.J. O'Brien, Macrophage polarization in response to collagen scaffold stiffness is dependent on cross-linking agent used to modulate the stiffness, ACS Biomater. Sci. Eng. 5 (2) (2019) 544–552.